Dynamical simulation of field emission in nanostructures

Seungwu Han,[1,2,*] M. H. Lee,[1] and Jisoon Ihm[1]

[1]*School of Physics, Seoul National University, Seoul 151-742, Korea*

[2]*Center for Strongly Correlated Materials Research, Seoul National University, Seoul 151-742, Korea*

(Received 4 April 2001; published 31 January 2002)

An efficient computational scheme based on the first-principles pseudopotential method is proposed for the electron emission from nanostructures under an applied electric field. The emission rate of the electron through the potential barrier is calculated by integrating the time-dependent Schrödinger equation for the states residing initially inside the emitter. Our approach takes into account the three-dimensional feature of the nanostructure as well as the realistic self-consistent potential. We have applied this method to the field emission of carbon nanotubes. The calculated emission currents are in good agreement with experimental data and exhibit strong dependence on the spatial distributions of the electronic wave functions.

I. INTRODUCTION

A strong electric field applied on the metal surface pulls out electrons from the metal via quantum-mechanical tunneling, which is called field emission. An analysis on the intensity of field-emitted electrons reveals valuable information such as the electronic structure of emitters or the variation of the work function as surface conditions change.[1] On the practical side, the field emission can be used in the display device by controlling the extracted electrons to hit a desired point of the phosphor screen. An array of field emitters replacing a bulky electron gun allows for a flat and thin display. Since the field-emission display operates at low temperatures, it consumes far less energy than the conventional display such as a cathode-ray tube that is based on thermal emission. These potential merits of the field-emission display have brought about industrial interests in developing a large-scale and energy-efficient display based on the field emission.

The metal emitters used for the field emission are usually designed to have a sharp edge in order to enhance the local electric field at the tip and achieve a high rate of electron tunneling. The radius of curvature of the emission tip has been typically around micrometers, but with the development in the fabrication technology and the advent of new materials, smaller tips with nanometer radius, namely, nanotips, begin to be used.[2] The nanotip is superior to the microtip in several ways. The most explicit advantage is the increase in the magnitude of the local electric field at the tip end, which results in the enhancement of the emission current compared to the microtip under the same external field. In addition, the low density of states at the tip makes the emitted electrons highly coherent and monoenergetic so that they can be used as an efficient source of the low-energy electron point source microscope.[3,4] The narrow opening angle of the electron beam is also suitable for a local probe of nanometric soft materials like RNA or carbon fibers.[2] The nanotip can be fabricated *in situ* with a field-ion technique on the metal surface: a local electric field greater than 1 V/Å rearranges the atoms that are mobile in the high-temperature condition, producing a nanometric protrusion on the flat-metal surface. On the other hand, there are also materials

generically retaining the geometric sharpness down to a nanometer scale. For example, the diameter of the carbon nanotube is only a few nanometers while its length can be extended up to several micrometers.

The current-voltage (I-V) characteristics of microtips are well described by the Fowler-Nordheim (F-N) theory developed in 1928.[5] This theory was formulated using the one-dimensional potential model with the free-electron-like metal of a given work function. The current I was calculated with the WKB approximation and its functional dependence on the bias voltage (V) is

$$I \propto V^2 \exp\left(-\frac{\phi^{3/2}}{\beta V}\right), \tag{1}$$

where ϕ is the work function and β is a constant proportional to the field enhancement factor. In most experimental situations, where the radius of curvature of the tip is greater than a micrometer, the I-V characteristics follow the form of Eq. (1), producing a straight F-N plot $[\ln(I/V^2)$ vs $1/V]$ and this is usually taken as evidence that the emission is driven by the field rather than by thermally excited electrons. The local electric field at the end of the tip is obtained from the slope of the F-N plot, using the known value of the work function. With its success in describing many experiments, the F-N theory has been the basic framework of many theoretical methods developed until now.

For studying the electronic behavior in the nanostructure, however, the simple picture of the F-N theory is not appropriate. First, the approximation of the tip as a square quantum-well potential is not justified at the nanometer scale since the concept of a sharp boundary between the emitter and the vacuum fails and the electronic structure significantly deviates from that of the simple quantum well. Second, the one-dimensional WKB approximation neglects the spatial variation of the wave function in the x-y plane (the emission is assumed to be in the z direction). The three dimensional character of the wave function becomes important in the nanotip because the x-y dimension of the tip is comparable to atomic distances. Third, it is well known that the adsorbate-induced localized states significantly change the emission current. The role of the localized states is pro-

nounced for the nanotip because the atomic size of the tip restricts the number of channels for extended states. The localized states are difficult to consider in the semiclassical approach because they are not the normally current-carrying states. These theoretical arguments are reinforced by experiments for nanotips showing anomalous results that are not clearly explained by the F-N theory. For example, the current from the nanotip is often saturated at the high voltage, resulting in a nonlinear F-N plot.[6,7] The peak position in the energy distribution of the emitted electron is fixed at the Fermi energy of the emitter in the F-N theory as observed in the experiment using microtips, but it shifts down in nanotips as the voltage increases.[8,9] In some experiments, the analysis based on the F-N model yields unreasonable work functions.[10,11]

The above observations strongly indicate that the study of the field emission of the nanostructure requires a more realistic quantum-mechanical treatment. There have been several attempts to go beyond the limit of the F-N theory: an accurate potential around the tip region has been obtained from the quantum-mechanical calculation or from the solution of the Laplace equation with a three-dimensional boundary of the tip.[12,13] However, the transmission functions in those methods are still evaluated in the one-dimensional method by employing the semiclassical approach along a specific line in the emission direction. Sophisticated quantum-mechanical methods have also been formulated and applied to relatively simple systems such as a flat-metal surface[14] or a single-atom tip.[15]

In the present paper, we propose a conceptually different scheme aiming at simulating the field emission of realistic nanostructures accurately. In the analysis of the field-emission process, we do not make any simplifying assumptions on the geometry, potential distributions, or electronic states. The transition (or tunneling) rate of the electron is evaluated by monitoring the time evolution of the wave function initially confined inside the emitter. We will describe the computational details below and then present the results for the field emission of carbon nanotubes as an example.

II. COMPUTATIONAL METHOD

For the convenience of explanation, we divide the system into three nonoverlapping regions along the emission direction: the emitter (S_{emt}), barrier (S_{bar}), and vacuum (S_{vac}) as shown in Fig. 1. The field-emission process can be thought as the transmission of the electron from S_{emt} to S_{vac} by tunneling through S_{bar}. Three steps in our approach for studying the field emission of nanostructures are explained below.

A. *Ab initio* tight-binding calculation

The first step is to obtain the self-consistent potential that drives the electron into the vacuum and the initial wave functions to be used in the time evolution. This is accomplished by an *ab initio* calculation for a finite cluster imitating the tip region of the nanostructure including the uniform external field ($E_{ext}\hat{z}$). The Hamiltonian in the pseudopotential formalism with the local-density approximation is composed of the
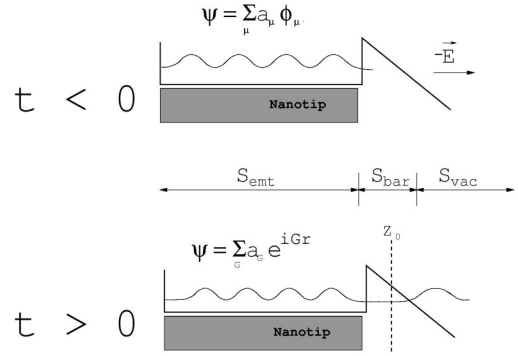

FIG. 1. Computational scheme for evaluating the transition rate of an electronic state. The wave function is described with the localized basis (ϕ_μ) before the transition ($t \le 0$). For $t > 0$, the basis is switched to plane waves (e^{iGr}) and the transition occurs. z_0 is the boundary used in evaluating the amount of the electron tunneling. S_{emt}, S_{bar}, and S_{vac} are the emitter, barrier, and vacuum regions, respectively.

kinetic operator T, the local potential V_L, and the nonlocal potential in the separable form proposed by Kleinman and Bylander (V_{NL}^{KB}),[16]

$$H = T + V_L + V_{NL}^{KB},$$

$$V_L = V_{Hxc}[\rho] - eE_{ext}z, \tag{2}$$

where V_{Hxc} is the Hartree and exchange-correlation potential evaluated from the electron density. The nonlocal term is a sum of potentials contributed from individual atoms.

$$V_{NL}^{KB} = \sum_{\tau lm} V_{NL}^{\tau lm} = \sum_{\tau lm} \frac{|\phi_{\tau lm}^0 V_{\tau l}\rangle\langle\phi_{\tau lm}^0 V_{\tau l}|}{Z_{\tau lm}}, \tag{3}$$

where l and m are indices for the angular and azimuthal momenta, respectively, $V_{\tau l}$ is the pseudopotential for the lth angular momentum of the τth atom, $\phi_{\tau lm}^0$ stands for the atomic orbitals, and $Z_{\tau lm}$ is the normalization factor.

In expanding wave functions, the localized orbitals are used

$$\psi_n^{loc}(\mathbf{r}) = \sum_{\mu\tau} a_{\mu\tau}^n \phi_{\mu\tau}(\mathbf{r} - \mathbf{R}_\tau), \tag{4}$$

where n is the band index, $\mathbf{R}_\tau$ is the position of the τth atom, and μ indicates the angular and azimuthal momenta. In this paper, the pseudoatomic orbitals are used for $\phi_{\mu\tau}(\mathbf{r})$.[17] By adopting the localized basis, the number of basis functions required for the calculation is reduced significantly. In addition, the finite radii of the basis naturally make the wave functions confined in S_{emt}. The standard pseudopotential method is employed and the self-consistent iteration is performed for the accurate description of the effect of external electric fields.

A practical issue here is a realistic modeling of the nanotip. When the height of the tip is within a nanometer, all atoms in the tip can be included in the computation.[8] In case of micron-long nanotips such as carbon nanotubes, however, millions of atoms are involved and quantum-mechanical cal-

culations would not be feasible for such a large system. The high aspect ratio in these materials amplifies the local electric field at the front of the emitter, making the tunneling process easier. In our previous study on the field emission of the carbon nanotube, it has been found that the local electric field at the tip of a very long nanotube can be simulated by applying a higher electric field on a shorter tube.[18] An important rule we have found there is that the charge accumulation at the tube end is essentially a function of the product of the tube length and the external electric field. Since the electrons are mainly emitted from the end of the nanotip, the realistic description of the local electric field in the vicinity of the end part of the nanotip is sufficient for evaluating the actual current in the experimental situation accurately. Thus, the effect of the large length can be taken into account by scaling the external electric field inversely to the length of the tip in the calculation. To reiterate, a short nanotube under a strong field may well simulate a long nanotube under a weak field as far as the emission is concerned.

B. Relaxation of the wave function

The wave functions expanded with the localized basis cannot extend into S_{vac} even though the potential of S_{vac} is lower than that of S_{emt}. To simulate the electron-emission process, the basis set is changed to plane waves. The coefficients of the plane waves are obtained from the inverse Fourier transform of the wave function in Eq. (4),

$$\psi_n^{PW}(\mathbf{r}) = \sum_{\mathbf{G}} a_{\mathbf{G}}^n \exp(i\mathbf{G}\cdot\mathbf{r}),$$

$$a_{\mathbf{G}}^n = \frac{1}{\Omega} \int \psi_n^{loc}(\mathbf{r})\exp(-i\mathbf{G}\cdot\mathbf{r})d\mathbf{r}, \tag{5}$$

where Ω is the volume of the supercell. The coefficients $\{a_{\mathbf{G}}^n\}$ are most easily obtained by projecting the nth eigenstate onto a regular grid and subsequently performing the inverse fast Fourier transformation.

Due to the incompleteness of the localized basis, the eigenstates calculated in the first step are slightly different from the exact ones. It causes a significant noise in the third step to be described later, making it difficult to assign a precise value for the transition rate. To circumvent this problem, we find it necessary to introduce a relaxation step adjusting the wave function inside S_{emt} to the exact eigenstate before calculating the time evolution of the wave function. As a measure of the deviation from the exact eigenstate, we calculate the norm of the residual vector δ defined as

$$\delta = \langle R | R \rangle,$$

$$|R\rangle = (H' - \langle\psi|H'|\psi\rangle)|\psi\rangle, \tag{6}$$

where the normalization of $|\psi\rangle$ is assumed. In order to prevent the escape of the electron into the vacuum during the relaxation, (note that everything is expanded in plane waves here) a strong repulsive potential (v_{rep}) is added for $z>z_0$ in the Hamiltonian

$$H' = H_{SC} + v_{rep}$$

$$v_{rep} = v_0 \theta(z-z_0), \tag{7}$$

where H_{SC} is the self-consistent Hamiltonian obtained in the first step. Here, z_0 effectively defines a boundary plane ($z = z_0$) perpendicular to the electric field separating the emitter and the vacuum.[19] v_0 of 1 Ry turns out to be sufficient for blocking the electron escape.

We have reduced δ by iteratively updating wave functions through the direct-inversion-in-the-iterative-subspace (DIIS) method, which we briefly recall in the following.[20] In the Nth DIIS step ($N\geq 3$), a normalized wave function $|\chi\rangle$ is constructed as a linear combination of the wave functions in the current iterative space

$$|\chi\rangle = \sum_{k=1}^{N-1} c_k|\psi^k\rangle. \tag{8}$$

The first and the second wave function in the iterative space are directly given by

$$|\psi^1\rangle = |\psi_n^{PW}\rangle,$$

$$|\psi^2\rangle = |\psi^1\rangle + \eta K|R^1\rangle, \tag{9}$$

where K indicates the preconditioning operation on the residual vector,[21] η is the size of the trial step (chosen as 0.3), and $|R^i\rangle = (H' - \langle\psi^i|H'|\psi^i\rangle)|\psi^i\rangle$. The coefficients $\{c_k\}$ of the Nth step in Eq. (8) are given by minimizing the norm of the residual vector of $|\chi\rangle$

$$|R_\chi\rangle = (H' - \langle\chi|H'|\chi\rangle)|\chi\rangle$$

$$= \sum_{k=1}^{N-1} c_k(H' - \langle\chi|H'|\chi\rangle)|\psi^k\rangle$$

$$\approx \sum_{k=1}^{N-1} c_k|R^k\rangle, \tag{10}$$

where the residual vector is assumed to be linear with the wave function. Minimizing the norm of $|R_\chi\rangle$ for the normalized $|\chi\rangle$ is equivalent to solving the generalized eigenvalue problem with $(N-1)$ dimensions

$$\sum_{j=1}^{N-1} \langle R^i|R^j\rangle c_j = \lambda \sum_{j=1}^{N-1} \langle\psi^i|\psi^j\rangle c_j, \tag{11}$$

where λ is the eigenvalue. The lowest eigenvector leads to the desired $\{c_k\}$, and hence $|R_\chi\rangle$ from Eq. (10). Then a new wave function $|\psi^N\rangle$ is introduced in the iterative space

$$|\psi^N\rangle = |\chi\rangle + \eta K|R_\chi\rangle, \tag{12}$$

with a subsequent normalization. If the norm of the residual vector of $|\psi^N\rangle$ is greater than a preset tolerance, the $(N+1)$th DIIS step is performed in the same manner. Since the array dimension of the wave function is enormous in a typical simulation of the field emission, the maximum size of the iterative space, N_{max}, is severely limited by the memory space of the computer. In that case, we restart the DIIS loop with the final state $|\psi^{N_{max}}\rangle$ as a new $|\psi^1\rangle$. In the DIIS method, information on other bands is not required for minimizing the residual vector of the specific state, and the time-

consuming orthogonalization process is avoided. For the original eigenstate constructed with the localized basis, δ is on the order of 0.1 a.u. and this is reduced below 0.001 a.u. after hundreds of DIIS steps. We find that $|\langle \psi^1 | \psi^{N_{max}} \rangle|^2$ is always greater than 0.9, meaning that the overall shape of the initial wave function does not change much during the relaxation.

C. Time evolution

The final procedure is to evaluate the transition rate of each state from S_{emt} to S_{vac} under the self-consistent potential calculated in the first step. For this, we monitor the motion of the electron by integrating the time-dependent Schrödinger equation

$$\psi_n^{PW}(\mathbf{r}, t+\Delta t) = \exp\left(-i\frac{H_{SC}}{\hbar}\Delta t\right)\psi_n^{PW}(\mathbf{r}, t), \quad (13)$$

where H_{SC} is the self-consistent Hamiltonian calculated in the first step. The initial wave function, $\psi_n^{PW}(\mathbf{r}, 0)$, has been set to the relaxed eigenstate in the second step. In solving Eq. (13), we adopt the split-operator method. The basic objective of the split-operator method is to separate the noncommutable operators in the exponent for a small time interval. In the second order of Δt, the exponent is decomposed into a symmetric form

$$\exp\left(\Delta t \sum_{j=1}^{q} A_j\right)$$
$$= \prod_{j=1}^{q} \exp\left(\frac{\Delta t}{2}A_j\right)\prod_{j=q}^{1}\exp\left(\frac{\Delta t}{2}A_j\right) + O(\Delta t^3), \quad (14)$$

where $\{A_i\}$ is a set of operators mutually noncommutable like kinetic and potential terms in H_{SC}. With the exponent of Hamiltonian in Eq. (2) separated following Eq. (14), the time-displacement operation can be efficiently carried out in the real and reciprocal spaces where the potential and kinetic operators are (semi)diagonal, respectively. The interchange between two spaces is easily realized by fast Fourier transformation. The order of the error caused by the splitting can be further reduced through a fourth-order decomposition suggested by Suzuki[22]

$$S_4(\Delta t) = \prod_{i=1}^{5} S_2(p_i\Delta t),$$

$$S_2(\Delta t) = \prod_{j=1}^{q} \exp\left(\frac{\Delta t}{2}A_j\right)\prod_{j=q}^{1}\exp\left(\frac{\Delta t}{2}A_j\right), \quad (15)$$

where the parameters p_i are chosen as

$$p_1 = p_2 = p_4 = p_5 = \frac{1}{4 - 4^{1/3}},$$

$$p_3 = 1 - 4p_1. \quad (16)$$

With the above scheme implemented into Eq. (13), we arrive at the following formula for the time evolution:[23]

$$\psi_n^{PW}(\mathbf{r}, t+\Delta t) \simeq S_4(\Delta t)\psi_n^{PW}(\mathbf{r}, t)$$
$$= \left[\prod_{i=1}^{5} S_2(p_i\Delta t)\right]\psi_n^{PW}(\mathbf{r}, t), \quad (17)$$

where S_2 in the present case is

$$S_2(x) = \exp\left[-\frac{1}{2}iTx\right]\left(\prod_{\tau lm}^{\text{ascending}}\exp\left[-\frac{1}{2}iV_{NL}^{\tau lm}x\right]\right)$$
$$\times \exp[-iV_L^{SC}x]\left(\prod_{\tau lm}^{\text{descending}}\exp\left[-\frac{1}{2}iV_{NL}^{\tau lm}x\right]\right)$$
$$\times \exp[-\frac{1}{2}iTx]. \quad (18)$$

The exponential of the nonlocal potential can be expressed analytically

$$\exp[xV_{NL}^{\tau lm}] = 1 + |P_{\tau lm}\rangle X_{\tau lm}\langle P_{\tau lm}|, \quad (19)$$

$$X_{\tau lm} = \frac{\exp\left[x\frac{\langle P_{\tau lm}|P_{\tau lm}\rangle}{Z_{\tau lm}}\right] - 1}{\langle P_{\tau lm}|P_{\tau lm}\rangle},$$

where $|P_{\tau lm}\rangle$ stands for $|\phi_{\tau lm}^0 V_{\tau l}\rangle$ in Eq. (3). As mentioned above, the kinetic operator is applied in the reciprocal space while the operations of nonlocal and local potentials are performed in the real space.

As time evolves, the electron starts to tunnel into S_{vac} and the electronic charge in S_{emt} begins to decrease. In order to evaluate the tunneling rate of the electron in the nth state, we integrate the square of the wave function for $z < z_0$

$$Q_n(t) = \int^{z_0}\int\int|\psi_n^{PW}(\mathbf{r}, t)|^2 dxdydz. \quad (20)$$

$Q_n(t)$ indicates the amount of the electron remaining in S_{emt} at time t. If we denote τ_n as a lifetime of the nth state, then we have

$$Q_n(t) = e^{-t/\tau_n}. \quad (21)$$

Equation (21) implies a linear behavior of Q_n in the short-time region, as will be demonstrated in Sec. III. The slope of the linear curve corresponds to the transition rate of the electron in the nth state of the emitter of the display device into the free traveling state that will ultimately hit the phosphor screen on the anode side.

There are many states contributing to the current and the total current of the nanotip is calculated as follows:

$$I = e\sum_n f_n\Gamma_n, \quad (22)$$

where f_n is the occupation number of the nth eigenstate in the model tip and Γ_n is its transition rate (inverse to the lifetime τ_n) estimated from the electron-tunneling (Q_n vs t) graph to be presented in Sec. III. Note that f_n as well as Γ_n
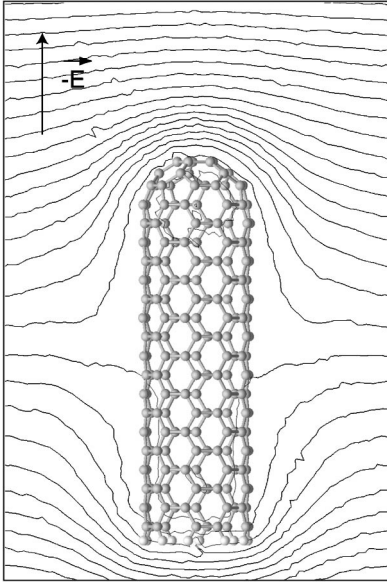
FIG. 2. Equipotential lines of the model system when the external field is 0.8 V/Å. Successive lines are separated by 1 V.

FIG. 3. Change of Q_n (the charge remaining in the nanotube) for a localized state as a function of elapsed time. The data are plotted for three different external fields (0.4, 0.6, and 0.8 V/Å).

generally depends on E_{ext}. Since the emission current mostly originates from the states within $1-2$ eV below the Fermi level, we only need to consider the time evolution of a fraction of states in the small energy window rather than the whole set of occupied states.

III. APPLICATION TO THE (5,5) CARBON NANOTUBE

The above method has been applied for studying the field emission of a carbon nanotube. The high aspect ratio and the mechanical strength inherent in the nanotube have opened a new class of materials for the electron emitters of the field-emission display.[24] However, the emission mechanism of the nanotube is still unresolved and many experimental findings remain to be clearly understood.[25] As a model system, we have used the (5,5) carbon nanotube[26] of 20 Å in length (see Fig. 2). Five pentagons are symmetrically placed around the circumference of the nanotube, closing the end of the nanotube with a hemisphere of C_{60}. The open end of the nanotube on the other side is passivated with hydrogen atoms. Troullier-Martins pseudopotentials[27] in the separable form with a cutoff energy of 40 Ry are employed and a supercell of 30 Å $\times$30 Å $\times$60 Å is used.

When the external field is applied, we find that the local field at the end of a particular tube is reduced significantly by the induced dipole moments in other supercells unless the lateral and vertical sizes of the supercell are much larger than the tube length. The electric field due to surrounding supercells could be explicitly summed and subtracted from the total field by simplifying the charge distribution in the unit supercell as a sum of multipole (up to quadrupole) moments centered at each atom. Figure 2 shows the difference between the self-consistent potentials with the external field of 0.8 V/Å and without it. It can be seen that the constancy of the potential is maintained over the nanotube surface, as expected from the metallicity of the (5,5) nanotube. The time
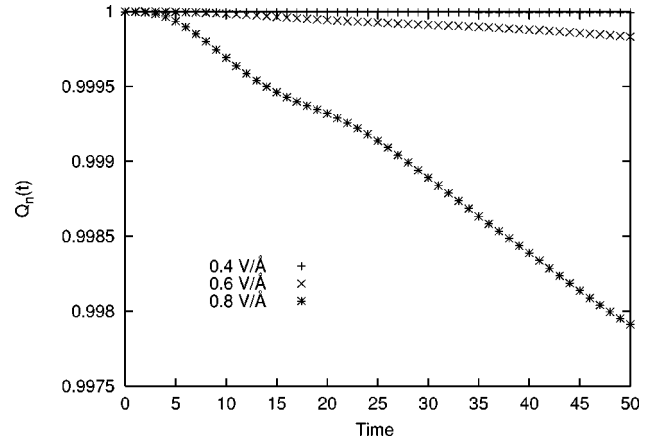
increment Δt in Eq. (13) is set to 0.1 a.u. (1 a.u.$=0.0242$ fs). In the time evolution of individual eigenstates, two types of states are identified with quite different transition rates; an extended state and a localized state. An extended state is distributed uniformly over the tube body while a localized state is confined within the cap region. It is well known that the topological defects such as pentagons in the (5,5)-capped nanotube generate localized states whose amplitudes decay exponentially away from the cap.[28]

Figure 3 shows the change of Q_n for a localized state as a function of time. It can be seen that the tunneling rate is greatly enhanced as the applied field increases. Since the change of Q_n right after the initiation of the tunneling process may depend on the position of z_0, we take a slope of Q_n in the time interval of 30 to 50 a.u. in evaluating the transition rate. The result is found to be insensitive to the choice of z_0. After a long time, the emitted electron is reflected by the artificial boundary of the supercell and flows backwards to the carbon nanotube. This artifact causes a resonance (Rabi oscillation) giving a large nonlinear change in Q_n. When we adopt a longer supercell, the initial time interval with the steady decrease of Q_n increases.[29] We evaluate the slope of Q_n well before the oscillation sets in. Note that the fraction of the wave function escaped from the emitter is less than 0.01 at the end of the simulation time ($\sim$ femtosecond) even for the highest field in Fig. 3, which means that the simulation time is very short compared to the lifetime of the state, τ_n. In a real situation, the empty state of the emitted electron will be replenished very fast (around femtosecond) by the extended states in the body of the nanotube overlapping with the localized states and the time lag due to the intratip transition from extended states to localized states is negligible compared with the rather slow process of tunneling (τ_n $\sim$ picosecond or slower).

In Fig. 4, computational results of the transition rates under the external field of 0.8 V/Å are displayed for the states within 2 eV below the Fermi level. It is striking that the transition rates of the localized states are far greater than those of the extended states. The origin of this pronounced current due to the localized state is revealed by inspection of
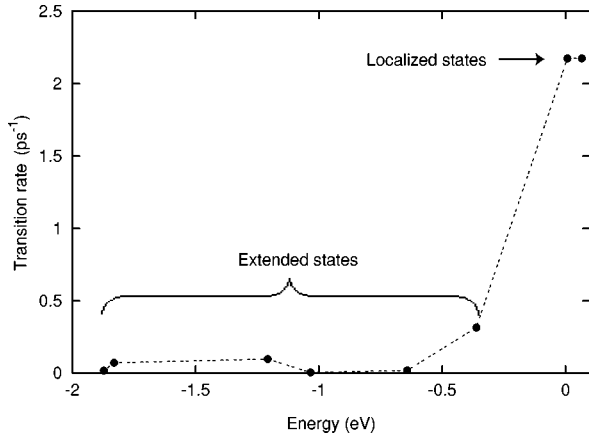
FIG. 4. Transition rates for the states within 2 eV below the Fermi level when the external field is 0.8 V/Å. The localized states are partially filled because of the Gaussian broadening of 0.1 eV used in the density of states.

its spatial distribution: The localized state is near the end of the nanotube where the local electric field is largest and the electron in this state can easily tunnel out to the vacuum. This is an exemplary case showing that the spatial distribution of the wave function as well as its energy level is important for the tunneling rate. The transition into the continuum state in S_{emt} implies broadening of the density of states and we estimate the intrinsic broadening of the localized states due to the tunneling transition to be as small as ~ 1.0 meV.

Figure 5 shows the computed I-E_{ext} curve for the model nanotube. The exponential growth of the current with respect to the external field is noticeable and the F-N plot presented in the inset is linear as predicted from the classical F-N formula. This indicates that the F-N formula provides a useful scheme for the purpose of the data fitting, although the F-N theory may not be strictly valid in nanostructures and the interpretation of the fitting parameters should be done with caution. It would be desirable to compare the calculated current with experimental data. However, a direct comparison with experiment is not feasible at present; the current in experiment is usually measured as a function of the applied
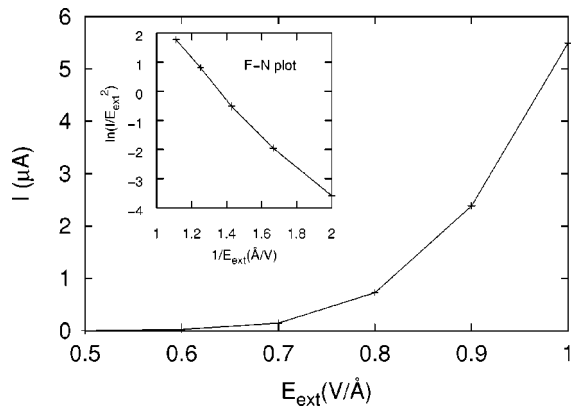

FIG. 5. Current-external field characteristics of the (5,5) nanotube. The inset is the F-N plot.

voltage and the relationship between the applied voltage and the electric field at the tip is complicated when the anode and cathode are not flat surfaces. (In case of the experiments performed with the flat anode and cathode, the uncertainty in the number of emission sites obscures an accurate comparison.) For a reasonable criterion for the comparison, we choose the effective local electric field (E_{loc}) evaluated from the F-N plot of I-E_{ext} (this work) or I-V (experiment) curves. From Fig. 5, the computed current is 100 nA when E_{loc} is 0.85 V/Å. (The work function of the carbon nanotube is assumed to be 5 eV.) In the experiment by Saito et al.,[30] the same amount of current was obtained when 1200 V was applied on the bundle of singlewall nanotube. The field enhancement factor (E_{loc}/V) measured from the F-N plot was 6.6×10^4 cm^{-1} on average which leads to E_{loc} of 0.79 V/Å, in good agreement with the above theoretical value.

IV. DISCUSSION

In summary, we have proposed a computational method suitable for studying the field emission of the nanosize structures very accurately. In this scheme, we obtain the potential and the starting wave functions with the localized basis at first and then calculate the transition rate through the time evolution of electrons with the plane wave basis. The localized basis in the first step naturally generates the wave function confined within the emitter and provides a realistic computational scheme for a large number of atoms in the unit cell. The rigorous computation of the currents of individual states in the present method is rather time consuming (since we are not employing simplifying schemes such as the WKB approximation), but one needs to consider only a small number of states near the Fermi level because of the exponential decay of the current as a function of the energy level. The realistic description of the system on the atomic scale enables us to study the detailed emission process based on the electronic structure of the emitter. In addition, this method allows a precise evaluation of the decay rate of the localized state. The implementation of the program using parameters given above (energy cutoff, external field, simulation time, etc.) produces stable results for the current between 10^{-1} and 10^4 nA, covering the practical range of the current from nanostructures. If necessary, the computational limit could be easily extended by increasing, say, the accuracy of the basis (i.e., energy cutoff).

We have also carried out the simulation starting with wave functions obtained in the absence of external electric field. (That is to say, the initial wave functions are exact eigenstates of the Hamiltonian for $t<0$.) The $Q_n(t)$ after applying electric field shows an oscillatory behavior but the rate of decrease on average is almost equal to the one evaluated from the present scheme. This indicates that the transition rate is largely insensitive to the small difference in the shapes of the wave functions with and without the external field. It is better to use the present scheme since the steady decrease of $Q_n(t)$ allows the evaluation of transition rate in a short time period.

It is interesting that the bound-to-continuum transition, which is the essential part of our calculation, has been widely

studied in semiconductor physics in conjunction with the dark current of the quantum well under the electric field. Theoretical methods there include the phase-shift method,[31] the complex-energy solution,[32] and the stabilization method.[33] They all focus on the calculation of the resonance width that gives the electron escape rate. Even though these methods have been limited to the study of one-dimensional quantum wells, the extended application to nanostructures may provide results comparable to our method.

In our calculation, the effect of the image charge has not been included. The image potential in nanostructures is certainly different from that in a simple metal plane. In our previous work,[34] the image potential was calculated for the nanotube by considering the electron-density change induced by an artificial potential of $-(1/r)$ (simulating the presence of a test electron) outside the tip. It was found that the screening by electrons in the nanotube gave qualitatively the same image potential but it was in general weaker than that of the classical result for the flat metal plane. This image potential will enhance the emission current by reducing the potential barrier in S_{bar} similar to the results of the F-N theory. A further analysis on this will be reported in the future.

*Present address: Princeton Materials Institute, Princeton University, Princeton, NJ 08544; Email: hansw@Princeton.EDU

[1] J. W. Gadzuk and E. W. Plummer, Rev. Mod. Phys. **45**, 487 (1973).

[2] For an extensive review, see V. T. Binh, N. Garcia, and S. T. Purcell, Adv. Imaging Electron Phys. **95**, 63 (1996).

[3] H. W. Fink, W. Stocker, and H. Schmid, Phys. Rev. Lett. **65**, 1204 (1990).

[4] W. Zhu, G. P. Kochanski, and S. Jin, Science **282**, 1471 (1998).

[5] R. H. Fowler and L. Nordheim, Proc. R. Soc. London, Ser. A **119**, 173 (1928).

[6] Vu Thien Binh, J. Microsc. **151**, 355 (1988); Vu Thien Binh and J. Marien, Surf. Sci. **202**, L539 (1988).

[7] P. G. Collins and A. Zettl, Phys. Rev. B **55**, 9391 (1997).

[8] Vu Thien Binh, S. T. Purcell, N. Garcia, and J. Doglioni, Phys. Rev. Lett. **69**, 2527 (1992).

[9] M. J. Fransen, Th. L. van Rooy, and P. Kruit, Appl. Surf. Sci. **146**, 312 (1999).

[10] I. Musa, D. A. I. Munindrasdasa, G. A. J. Amaratunga, and W. Eccleston, Nature (London) **395**, 362 (1998).

[11] A. N. Obraztsov, A. P. Volkov, aand I. Yu. Pavlvoskii, JETP Lett. **68**, 59 (1998).

[12] J. He, P. H. Cutler, and N. M. Miskovsky, Appl. Phys. Lett. **59**, 1644 (1991).

[13] A. Lorenzoni, H. E. Roman, F. Alasia, and R. A. Broglia, Chem. Phys. Lett. **276**, 237 (1997).

[14] Y. Gohda, Y. Nakamura, K. Watanabe, and S. Watanabe, Phys. Rev. Lett. **85**, 1750 (2000).

[15] N. D. Lang, A. Yacoby, and Y. Imry, Phys. Rev. Lett. **63**, 1499 (1989).

[16] L. Kleinman and D. M. Bylander, Phys. Rev. Lett. **48**, 1425 (1982).

[17] O. F. Sankey and D. J. Niklewski, Phys. Rev. B **40**, 3979 (1989); the cutoff radius is set to 4.0 a.u. for C and H atoms.

[18] S. Han and J. Ihm, Phys. Rev. B **61**, 9986 (2000).

[19] A reasonable choice of z_0 would be the classical turning point of the state. For example, for a state 5 eV below the vacuum level, z_0 is 5 Å from the outermost atom if the local electric field is equal to 1 V/Å.

[20] G. Kresse and J. Furthmüller, Phys. Rev. B **54**, 111 169 (1996).

[21] M. P. Teter, M. C. Payne, and D. C. Allan, Phys. Rev. B **40**, 12 255 (1989).

[22] M. Suzuki, Phys. Lett. A **146**, 319 (1990).

[23] O. Sugino and Y. Miyamoto, Phys. Rev. B **59**, 2579 (1999).

[24] W. B. Choi, D. S. Chung, J. H. Kang, H. Y. Kim, Y. W. Jin, I. T. Han, Y. H. Lee, J. E. Jung, N. S. Lee, G. S. Park, and J. M. Kim, Appl. Phys. Lett. **75**, 3129 (1999).

[25] J.-M. Bonard, J.-P. Salvetat, T. Stockli, L. Forro, A. Chatelain, Appl. Phys. A: Mater. Sci. Process. **69**, 245 (1999).

[26] N. Hamada, S. I. Sawada, and A. Oshiyama, Phys. Rev. Lett. **68**, 1579 (1992).

[27] N. Troullier and J. L. Martins, Phys. Rev. B **43**, 1993 (1991).

[28] R. Tamura and M. Tsukada, Phys. Rev. B **52**, 6015 (1995).

[29] For an even longer vaccum and simulation time, we observe that the slope reduces continuously, which is a signature of exponential decay.

[30] Y. Saito, K. Hamaguchi, R. Mizushima, S. Uemura, T. Nagasako, J. Yotani, and T. Shimojo, Appl. Surf. Sci. **146**, 305 (1999).

[31] E. J. Austin and M. Jaros, Phys. Rev. B **31**, 5569 (1985).

[32] D. Ahn and S. L. Chuang, Phys. Rev. B **34**, 9034 (1986).

[33] V. A. Mandelshtam, T. R. Ravuri, and H. S. Taylor, Phys. Rev. Lett. **70**, 1932 (1993).

[34] J. Ihm and S. Han, in *Science and Application of Nanotubes (Fundamental Materials Research)*, edited by D. Tomanek and R. J. Enbody (Plenum Press, New York, 2000).